Pergamon

Int. J. Heat Mass Transfer. Vol. 40, No. 9, pp. 2123–2131, 1997

0017-9310/97 $17.00+0.00

PII: S0017-9310(96)00267-0

A critical heat flux correlation for droplet impact cooling

M. L. SAWYER,† S. M. JETER and S. I. ABDEL-KHALIK‡

George W. Woodruff School of Mechanical Engineering, Georgia Institute of Technology, Atlanta, GA 30332, U.S.A.

(*Received* 28 *March* 1996 *and in final form* 12 *July* 1996)

Abstract—The characteristics of a single stream of monodispersed water droplets impacting a horizontal, upward facing flat surface have been investigated. The objective was to determine the effect of droplet diameter, impact frequency and impact velocity on the critical heat flux (CHF). A generalized correlation has been developed for the nondimensional CHF as a function of the Weber and Strouhal numbers of the impacting droplets. The Weber and Strouhal numbers ranged from 175 to 730 and 7.00×10^{-3}–3.00×10^{-2}, respectively. With a confidence level of greater than 95% differences between predicted and experimental CHF values were less than ±22%. © 1997 Elsevier Science Ltd. All rights reserved.

INTRODUCTION

Extremely high heat fluxes can be dissipated when a surface is impacted by a spray or a stream of liquid droplets. Common systems involving droplet impact heat transfer include the evaporation of fuels in automobile injection systems and the quenching of metals in foundries. Droplet impact cooling may prove effective in cooling electronic components, high power lasers and the leading edges of high speed aerospace craft. Droplet cooling promises significantly higher heat fluxes than conventional alternatives such as pool boiling. However, its application presents additional complexities associated with droplet generation and impact, as well as the evaporation and stability of the resulting liquid layer.

Droplet impact cooling can be subdivided into two categories: (1) sprays; and (2) single streams of uniform, or monodispersed, droplets that strike a spot in sequence. In either category, droplet cooling provides high heat flux through the continuous formation and evaporation of a thin liquid film on a hot surface. Several studies of both categories have been undertaken, an extensive literature review is given in Ref. [2]. Streams of monodispersed droplets provide a more simplified approach to understanding the basic characteristics of droplet cooling. Still, several investigators have studied sprays. Among these are Toda [3], Bonacina *et al.* [4], Tilton and Chow [5], and Pais *et al.* [6].

Other investigators have chosen to study droplet streams. A few of the early experiments were carried out by Wachters and Westerling [7], McGinnis and Holman [8] and Pedersen [9]. Another work is that of Valenzuela *et al.* [10, 11]. Using droplets of about 91 μm, they achieved a critical heat flux (CHF) of 324 W cm^{-2} at a wall superheat (i.e. $T_{wall} - T_{sat}$) of 37°C. More recently, Halvorson *et al.* [12, 13] examined the effect of impact frequency, subcooling and ambient pressure on the CHF for large (3–4 mm) droplets.

The objective of the present investigation was to empirically examine the effects of droplet diameter, impact frequency, and velocity on the critical heat flux for a horizontal, upward facing flat surface. The aim was to identify trends leading to CHF enhancement and to develop a generalized correlation for CHF as a function of the relevant parameters.

EXPERIMENTAL APPARATUS

The experimental apparatus used in this investigation consists of three systems. These include a heater system, an instrumentation system and a fluid delivery system. The fluid delivery system was designed to provide a single stream of monodispersed water droplets to the heat transfer surface. The system was designed so that each parameter, namely, impact frequency, velocity and droplet diameter, i.e. mass flow rate, could be varied independently while the others are kept constant. This design allowed the effect of each parameter on CHF to be clearly identified. Thermocouples within the heater monitor the resulting heat transfer, which is recorded via a computer-based data acquisition system. The heater, instrumentation and fluid delivery systems are described below.

Heater

The primary component of the heater system is an internally heated copper cylinder, illustrated in Fig. 1,

† Present address: AlliedSignal, Inc., Petersburg, VA 23804, U.S.A.

‡ Author to whom correspondence should be addressed.

NOMENCLATURE

CHF	critical heat flux [W cm^{-2}]
CHF_k^*	Kutateladze number [1] used to nondimensionalize adjusted CHF according to equation (3)
c_p	specific heat [J (kg·°C)$^{-1}$]
d	droplet diameter before impact [mm]
D	maximum diameter to which a droplet initially spreads after impact [mm]
f	frequency of the impacting droplets [Hz]
h_{fg}	heat of vaporization of liquid water [J kg^{-1}]
$\dot{m}$	mass flow rate of water [kg s^{-1}]
PTFE	polytetrafluoroethylene (Teflon®)
$\dot{Q}$	rate of heat transfer [W]
Re	Reynolds number for falling droplet $(\rho_L \cdot v_i \cdot d/\mu_L)$
St	Strouhal number for the impacted droplet $(f \cdot d/v_i)$
T	temperature [°C]
v	velocity of droplet [m s^{-1}]
We	Weber number for falling droplet $(\rho_L \cdot v_i^2 \cdot d/\sigma_L)$.

Greek symbols

β	spreading ratio for impacting droplet (D/d)
μ	dynamic viscosity of water [kg (m·s)$^{-1}$]
ρ	density [kg m^{-3}]
σ	surface tension of water [N m^{-1}].

Subscripts

i	at impact, measured normal to the surface of impact
L	liquid, at room temperature
sat	at saturation
wall	at heat transfer surface or at temperature of heat transfer surface
water	supply water.

whose upper, horizontal face acts as a heat transfer surface for the impacting water droplets. The 17 kg copper cylinder provides a conductive path between four cartridge heaters and the heat transfer surface. The cylinder is 30.5 cm (12 inches) in total length. It is 10.2 cm (4 in.) in diameter at its base and tapers to a 1.5 cm diameter region, which ends at the heat transfer surface. The reduced diameter increases the heat flux passing through the upper surface. The heater system was previously used by Bockwoldt *et*

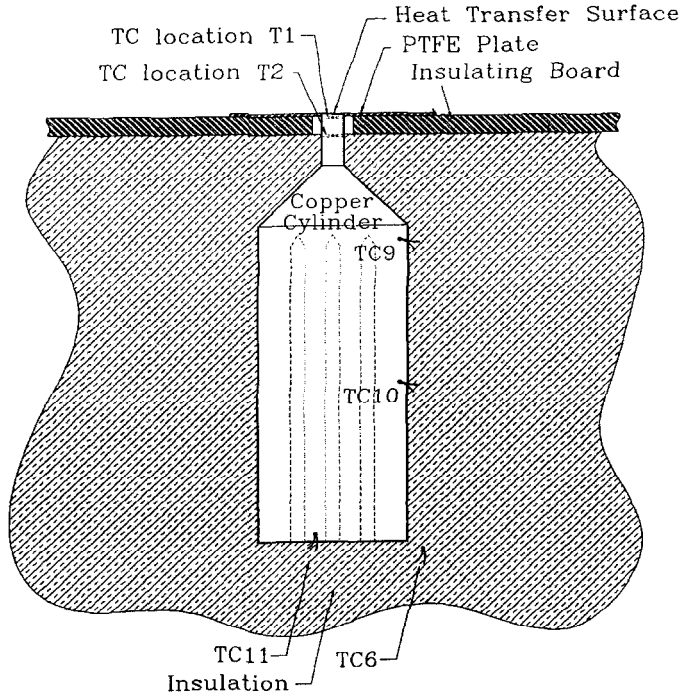

Fig. 1. Schematic of the heated copper cylinder showing its thermocouple locations. The height is 30.5 cm; the heat transfer surface is 1.5 cm in diameter.

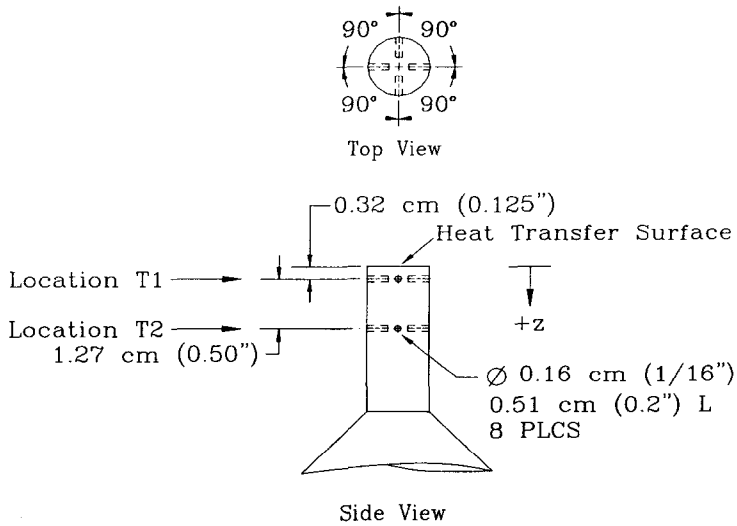

Fig. 2. The upper region of the heated copper cylinder with the thermocouple locations of the heat rate calorimeter shown.

al. [14] and Messana [15]. An electrical power input of 1800 W was used for the experiments. The power is consumed in three ways: heat transfer to the droplets, heat storage in the cylinder and heat loss to the surroundings. The power delivered to each of these three 'sinks' is measured with the aid of numerous thermocouples installed throughout the cylinder. Thermocouples at two elevations directly beneath the heat transfer surface form a heat rate calorimeter. These locations are designated as T1 and T2 in Fig. 2. The calorimeter monitors the temperature of the surface and the heat transferred to the impacting droplets. Level T1 contains two thermocouples 180° apart, 0.32 cm (1/8 in.) below the heat transfer surface. Level T2 contains three thermocouples 90° apart, 1.59 cm (5/8 in.) below the heat transfer surface. All thermocouples are inserted to a radial depth of 0.51 cm (0.20 in.) from the outer edge of the reduced diameter region (i.e. approximately 0.24 cm from the centerline).

An insulated box houses the cylinder. To inhibit water from flowing along the side of the cylinder, a 0.32 cm (1/8 in) PTFE plate is tightly fitted beneath the edge of the heat transfer surface. Originally, white PTFE was used, but graphite-impregnated black PTFE was found to provide a far superior background for the video images.

Prior to the experiments, the heat transfer surface was nickel plated to provide corrosion resistance and to stabilize its performance. The surface was cleaned, on the average, once every 10 experiments with a strong surfactant followed by an acetone rinse. The use of distilled water during the experiments prevented minerals from being deposited on the surface. The suitability and corrosion resistance of the nickel plating was verified by conducting 'control experiments', i.e. experiments with identical conditions. These control experiments were executed in order to confirm the consistency and repeatability of the data and to monitor the possible effect of the aging of the heat transfer surface. Eleven control experiments were interspersed among the 71 total experiments reported herein. The system performed consistently with 90% confidence bands of only $\pm 14\%$, as measured with respect to the mean of the entire control set.

Instrumentation

The instrumentation consists of a data acquisition system (Keithley-Metrabyte DAS-8 and EXP-16) installed in a personal computer and thermocouples located throughout the heater. A gain of 200 on the system's instrumentation amplifier provides a resolution of ± 0.3°C. Data are recorded to disk via a BASIC program which consists of vendor-supplied subroutines and a user interface developed by Halvorson [12]. The program allows the user to monitor temperatures throughout the heated cylinder and to observe heat transfer results during an experiment. To reduce the influence of random fluctuations, 30 thermocouple readings are averaged for each data point. The averaged thermocouple readings are recorded every 3 s.

Fluid delivery

The goal of the fluid delivery system was to produce a single continuous stream of monodispersed water droplets. A schematic of the entire fluid delivery system is presented in Fig. 3. With this system, droplet impact frequency, velocity and diameter, i.e. mass flow rate, can be varied independently. The overall range of parameters obtained with the fluid delivery system is given in Table 1.

The fluid delivery system consists of three parts: a liquid supply, a droplet generator and a selector wheel. The liquid supply provides a constant-pressure source of liquid for the droplet generator. Constant pressure is achieved by using an over-flowing water reservoir. The generator was designed based on Rayleigh's analysis of the break-up of a cylindrical liquid jet

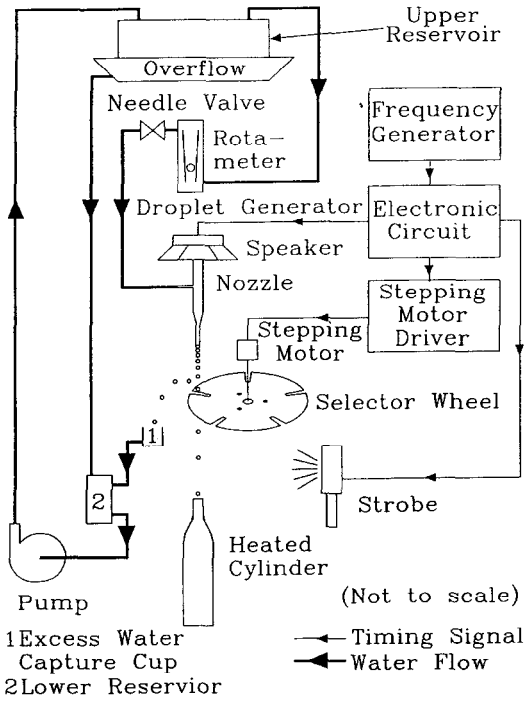

Fig. 3. The fluid delivery system.

[16, 17]. A single, continuous stream of uniform or monodispersed water droplets is produced by forcing a nozzle with an audio speaker coil. The coil is driven by a fixed frequency square wave. The forcing frequency dictates the droplet production frequency. The impact velocity of the droplets is controled by varying the elevation of the generator relative to the heated surface and is calculated using the equation for a free-falling object.

Because the generator produces an excess quantity of droplets, a slotted, rotating disk, referred to as a selector wheel, has been built to meter the droplets. The selector wheel is placed between the droplet generator and the heat transfer surface and is driven by a stepping motor. Only a prescribed fraction of the droplets pass through the slots of the wheel; the remainder strike the wheel and are recirculated. To maintain a consistent time and phase relationship, a single source ultimately clocks both the stepping motor driver and the droplet generator, as indicated in Fig. 3. The stepping motor driver is clocked at one-half the frequency of signal source. The same source frequency is divided by 10 with a walking ring counter and is then amplified before reaching the generator.

Table 1. Range of experimental parameters

impact velocity	2.4–4.6 m s^{-1}
impact frequency	12–42 Hz
droplet diameter	1.5–2.7 mm
mass flow rate	79 and 194 mg s^{-1}
Weber number	175–730
Strouhal number	7.00×10^{-3}–3.00×10^{-2}

The 5 : 1 ratio between the two signals keeps the selector wheel and the droplet generator properly synchronized. The walking ring counter maintains the 50% duty cycle of the source signal. The original droplet generator and selector wheel were based on designs by Messana [15]. Other designs were developed and built to achieve the required range of parameters and to improve performance. Aided by the digital 'gearing' and the amplification of a specialized electronic circuit, the liquid supply, droplet generator, and selector wheel perform as an integrated fluid delivery system, producing a continuous stream of monodispersed droplets. Additional details regarding the design and operation of the experimental apparatus may be found in Ref. [2].

RESULTS AND DISCUSSION

CHF trends

Single stream droplet impact cooling experiments were conducted in the low superheat regime and were concluded when the critical heat flux was reached. Distilled water at room temperature, 25°C, was used. The parameter set has been previously provided in Table 1. With the apparatus used, droplet impact frequency, velocity and diameter, i.e. mass flow rate, were varied independently. This independence of all three parameters is unique as compared to most other experiments. Trends were compiled by varying a single parameter from one experiment to the next, and a generalized correlation for the normalized CHF was obtained.

An experiment begins by adjusting the droplet production system to provide the desired impact frequency, velocity and droplet diameter. The heaters within the copper cylinder are energized and the cylinder temperature begins to rise. Initially, the heat transfer surface is near the saturation temperature of the liquid. Little heat is removed by the impacting droplets and most of the energy input is stored within the cylinder. As the surface temperature rises, the heat flux to the impacting droplets rises and nucleate boiling is observed. Eventually the temperature and heat flux rise to the point that the droplets can no longer wet and spread across the surface. At that point heat flux plummets and the surface temperature rapidly increases. The maximum heat flux achieved just prior to this cooling crisis is the critical heat flux (CHF). Once the CHF is achieved, the experiment is terminated.

CHF represents the uppermost limit of low temperature, two-phase heat transfer from the thin liquid film formed by droplet impact. Hence, understanding the limits of droplet impact cooling and knowing how to maximize these limits are essential aspects of applying this technique in a practical system. During each experiment, the surface-averaged CHF was obtained using the heat rate calorimeter located beneath the surface of the cylinder. The heat flux was calculated from the temperature gradient near the heat transfer

surface as measured by the average temperatures at the T1 and T2 elevations (Fig. 2). One-dimensional heat flow was assumed. The limits of uncertainty for the measured heat flux were evaluated based on the uncertainties in the thermocouple readings, the location of the thermocouples, and the thermal conductivity of the copper. The total uncertainty in the thermocouple readings was $\pm 1.37°C$, the uncertainty in the location of the thermocouples was ± 0.045 cm, and the uncertainty in the thermal conductivity was estimated to be 0.085 W (cm °C)$^{-1}$. These values were combined by error propagation analysis to obtain the predicted limits of accuracy for the measured heat flux. Based on this analysis, the uncertainty in thermocouple location was the major contributor. The resulting limits of accuracy were ± 7.7 W cm^{-2} or $\pm 5\%$ for the surface-averaged CHF of a typical experiment. Surface-averaged CHF values ranged from 52.0 to 203.1 W cm^{-2} while the heat transfer effectiveness at CHF ranged from 0.55 to 0.94. The effectiveness measures the actual rate of heat transfer to the droplet stream as compared to the maximum rate of heat transfer possible for the given mass flow rate:

$$\text{effectiveness} = \frac{\dot{Q}_{\text{wall}}}{\dot{m}(h_{\text{fg}} + c_{\text{pL}}(T_{\text{sat}} - T_{\text{water}}))}. \quad (1)$$

Experimental data indicate that the surface-averaged heat flux, i.e. heat flux based on the entire heat transfer surface irrespective of what fraction is actually wetted by the droplets, is insensitive to both droplet impact frequency and velocity. The surface-averaged CHF does, however, increase with the mass flow rate. Clearly, for a given set of parameters, the surface-averaged heat flux will depend on the system design, i.e. the size of the heat transfer surface itself. Therefore, it is inappropriate to present the data in such a form since they could not be universally applied. Additionally, the droplet impact frequency and velocity affect the heat transfer process by influencing the spreading and stability of the resulting liquid film. Therefore, the surface-averaged CHF, which is insensitive to these parameters, may not be the best tool for measuring droplet heat transfer performance.

Due to the apparent inadequacy of surface-averaged CHF to fully characterize droplet heat transfer, an improved parameter was sought. As higher superheats are achieved, the evaporation rate increases, and portions of the surface become dry between droplets. During this period, the outer region of the surface remains dry because an individual droplet does not typically spread across the entire surface. Radiation and convection from the dry regions are negligible. The size of the wetted region varies as droplet size and impact velocity are varied from one experiment to the next. Therefore, adjusting the CHF to account for the partial wetting of the surface is appropriate. The 'adjusted' CHF is calculated using an estimate of the maximum area initially wetted after a droplet impacts and spreads across the heat transfer surface. With portions of the surface remaining dry, the adjusted CHF is clearly the preferred parameter for performance comparisons since any practical design would include an array of appropriately spaced nozzles. Additionally, presentation of the CHF based on the initially-wetted area would be universally applicable regardless of the size of the experimental heat transfer surface itself.

To facilitate the calculation of initially-wetted area and the corresponding values for the adjusted CHF, an equation originally formulated by Kurabayashi and later improved by Yang [18] has been employed:

$$\frac{1}{2}We = \frac{3}{2}\beta^2\left[1 + 3\frac{We}{Re}\left[\frac{\mu_{\text{L}}}{\mu_{\text{wall}}}\right]^{0.14} \times \left[\beta^2 \ln(\beta) - \frac{\beta^2 - 1}{2}\right]\right] - 6. \quad (2)$$

This equation implicitly calculates the droplet spreading ratio, β, in terms of the Weber and Reynolds numbers of the impacting droplet. The spreading ratio is defined as the ratio of the diameter of maximum spread after impact to the diameter of the droplet before impact. Equation (2) assumes that the impacting droplets spread to form disks of uniform thickness. From the spreading ratio the wetted area may be estimated. The predicted spreading ratios from the above equation have been found to be in excellent agreement with observed values over a wide range of Weber and Reynolds numbers [11–13, 19]. In the event that the droplets were predicted to spread beyond the heat transfer surface, the total area of the surface was used to calculate the adjusted CHF.

The adjusted CHF increases monotonically with increased droplet frequency as shown Fig. 4. Droplet frequency dictates droplet diameter when the mass flow rate is held constant. Higher frequencies result in smaller droplets, which spread to thinner films as predicted by equation (2). Higher heat fluxes are anticipated for thinner films [10–13] and, so, the relationship between adjusted CHF and frequency follows the expected trend. Figure 5 shows the frequency results for all the experimental data while Fig. 4 presents the results for a single value mass flow rate and three different impact velocities.

The data indicate that the adjusted CHF declines when the impact velocity is increased, opposite to the trend expected for the thinner films produced. This trend is shown for three different frequencies in Fig. 6 and two different mass flow rates in Fig. 7. Perhaps higher velocities substantially affect the uniformity and stability of the liquid film formed by droplet impact.

In this experiment, the impact velocities ranged from 2.4 to 4.6 m s^{-1} and Weber numbers ranged from 175 to 730. The Weber number provides a measure of the relative strengths of the competing effects of surface tension and inertial forces. Its significance in

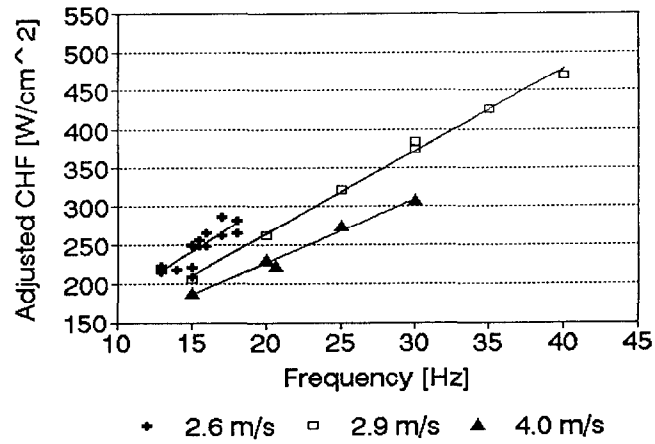

Fig. 4. Effect of droplet impact frequency on the adjusted CHF. Mass flow rate = 142 mg s^{-1}.

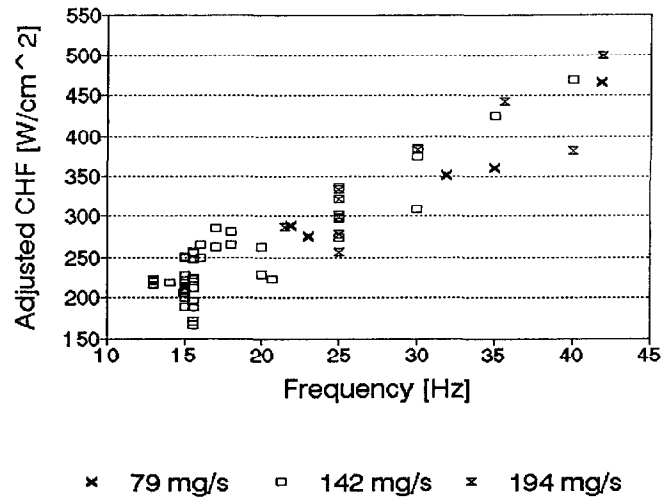

Fig. 5. Adjusted CHF for all experiments plotted against impact frequency. Several impact velocities are represented.

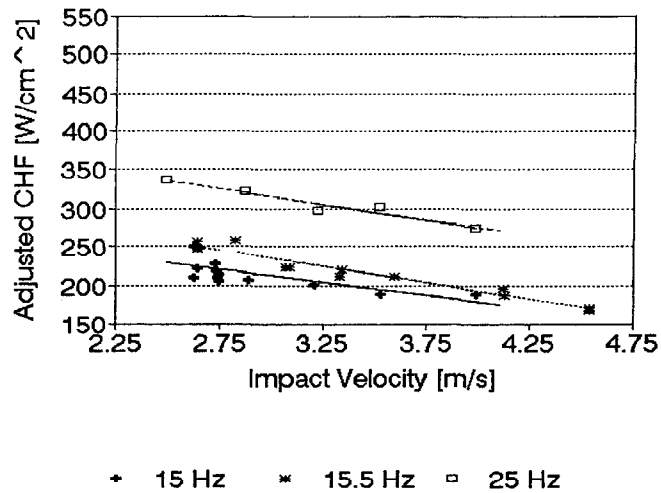

Fig. 6. Effect of droplet impact velocity on the adjusted CHF. Mass flow rate = 142 mg s^{-1}.

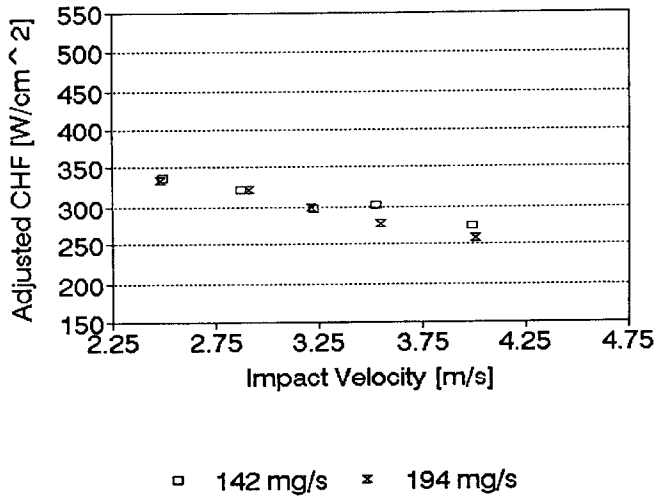

Fig. 7. Effect of droplet impact velocity on the adjusted CHF. Impact frequency = 25 Hz.

characterizing the droplet impact process was recognized by Watchers and Westerling [7]. Although their work focused on the high temperature, non-wetting regime, the basic concepts are appropriate to the low temperature regime as well. Therefore, the Weber number is expected to provide a measure of the effect of impact velocity.

CHF correlation

A generalized correlation which allows the adjusted CHF to be determined for a given set of conditions has been developed. In developing this correlation, we were guided by the CHF correlation reported by Monde and Inoue [1] for a surface impacted by a liquid jet. While jet impact cooling differs significantly from droplet impact cooling, they share some of the important physical features, namely, the formation and evaporation of a thin liquid film formed upon impact with a heated surface. The Kutateladze number is used to nondimensionalize the adjusted CHF data as suggested by Monde and Inoue [1]:

$$\mathrm{CHF}_{\mathrm{k}}^{*}=\frac{\mathrm{CHF}^{*}}{\rho_{\mathrm{L}} h_{\mathrm{fg}} v_i}. \tag{3}$$

The independent variables in this case are the Weber and Strouhal numbers, which incorporate the characteristic parameters of droplet impact cooling:

$$We=\frac{\rho_{\mathrm{L}} v_i^2 d}{\sigma_{\mathrm{L}}} \tag{4}$$

and

$$St=\frac{fd}{v_i}. \tag{5}$$

Least squares fitting of the data results in the following correlation:

$$\frac{\mathrm{CHF}^{*}}{\rho_{\mathrm{L}} h_{\mathrm{fg}} v_i}=0.1660 We^{-0.4138} St^{0.8906}. \tag{6}$$

Figure 8 demonstrates the ability of equation (6) to characterize the entire CHF data set. The coefficient of determination was 0.9637, indicating that 96% of the variation in the data is predicted by the correlation. The limits of accuracy describing the difference between the predicted and experimental non-dimensionalized adjusted CHF values was less than 22%. Figure 9 provides a direct comparison between the experimental and predicted data. These results indicate that equation (6) provides a reasonable correlation between the CHF data and the parameters most significant to droplet impact cooling, namely impact frequency, impact velocity and droplet diameter. Furthermore, using the wetted area to evaluate the CHF makes the results invariant with respect to the heat transfer area. So, although the correlation was developed for a single stream, it may be applicable to multiple, non-interacting, streams impacting simultaneously. The data on which equation (6) is based cover the following ranges of Weber and Strouhal numbers:

$$175 \leqslant We \leqslant 730$$

and

$$7.00\times 10^{-3} \leqslant St \leqslant 3.00\times 10^{-2}. \tag{7}$$

CONCLUSIONS

An experimental study has been carried out to investigate the effect of various parameters on the critical heat flux for a single stream of monodispersed water droplets. Adjusted CHF values of nearly 500 W cm^{-2} have been achieved at superheats of only 20°C. During the study, droplet impact frequency, velocity and diameter were independently varied. For the range of parameters examined, the surface-averaged CHF is insensitive to droplet impact frequency and velocity. In contrast, the physically-more-significant

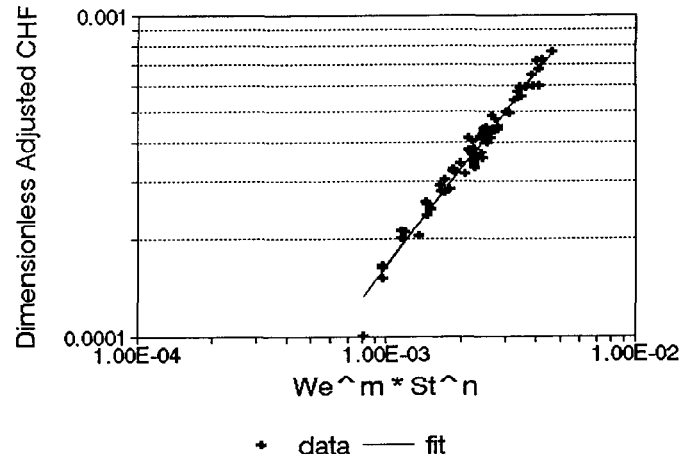

Fig. 8. Correlation between the Weber and Strouhal numbers and the dimensionless adjusted CHF. The correlation is defined in equation (6).

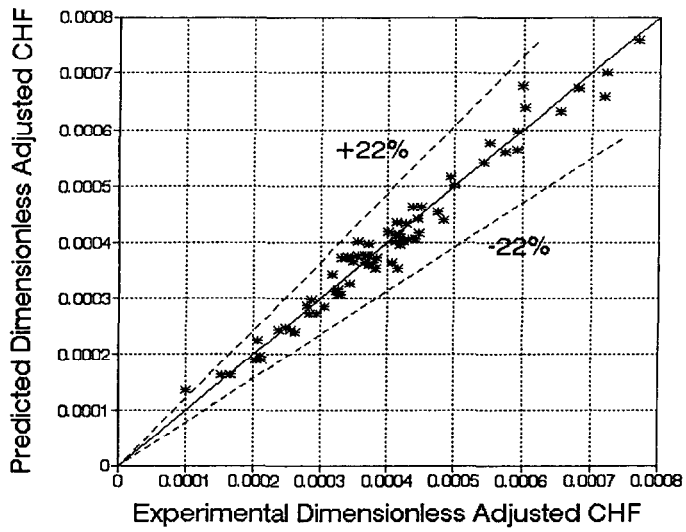

Fig. 9. Comparison between the predicted and experimental data as evaluated with the correlation defined in equation (6).

adjusted CHF, based on the initially-wetted area, increases significantly with impact frequency but declines with increased impact velocity. The results suggest that increased impact frequency is advantageous in maximizing CHF, but increased impact velocity may not be. The CHF results were evaluated and a generalized correlation was developed. Equation (6) is the main result of this work: it allows the critical heat flux to be evaluated for any combination of droplet impact frequency, velocity and diameter.

The limits of accuracy for the developed correlation were less than 22%. Using the wetted area to evaluate the CHF makes the results invariant with respect to the heat transfer area. So, although the correlation was developed for a single stream, it may be applicable to multiple streams impacting simultaneously.

REFERENCES

1. Monde, M. and Inoue, T., Critical heat flux in saturated forced convective boiling on a heated disk with multiple impinging jets. *ASME Journal of Heat Transfer*, 1991, **113**, 722–727.
2. Sawyer, M. L., High intensity heat transfer to a stream of monodispersed water droplets. Ph.D. thesis, Georgia Inst. of Technology, School of M.E., Atlanta, GA, 1996.
3. Toda, S., A study of mist cooling, 2nd report: theory of mist cooling and its fundamental experiments. *Heat Transfer—Japanese Research*, 1974, **3**(1), 1–44.
4. Bonacina, C., Del Giudice, S. and Comini, G., Dropwise evaporation. *ASME Journal of Heat Transfer*, 1979, **101**(3), 441–446.
5. Tilton, D. E. and Chow, L. C., High power density evaporative cooling, AIAA-87-1536, *22nd Thermophysics Conference*, American Inst. of Aeronautics and Astronautics, Honolulu, Hawaii, 1987, pp. 1–6.
6. Pais, M., Tilton, D. and Chow, L., High heat flux, low superheat evaporative spray cooling, AIAA-89-0241, *27th Aerospace Sciences Meeting*, American Inst. of Aeronautics and Astronautics, Reno, Nevada, 1989, pp. 1–10.
7. Watchers, L. H. J. and Westerling, N. A. J., The heat transfer from a hot wall to impinging water drops in the spheroidal state. *Chemical Engineering Science*, 1966, **21**, 1047–1056.

8. McGinnis F. K. and Holman, J. P., Individual droplet heat transfer rates for splattering on hot surfaces. *International Journal of Heat and Mass Transfer*, 1969, **12**, 95–108.
9. Pedersen, C. O., An experimental study of the dynamic behavior and heat transfer characteristics of water droplets impinging upon a heated surface. *International Journal of Heat and Mass Transfer*, 1970, **13**, 369–381.
10. Valenzuela, J. A., Jasinski, T. J. and Drew, B. C., High flux evaporative cold plate for space applications: phase I final report, TM-1103, NASA Contract NAS9-17574, Creare Inc., Hanover, New Hampshire, 1986.
11. Valenzuela, J. A. and Drew, B. C., High heat flux droplet impingement heat transfer: phase I final report, TM-1190, NSF Grant no. ISI 8660953, Creare Inc., Hanover, New Hampshire, 1987.
12. Halvorson, P. J., On the heat transfer characteristics of spray cooling. Ph.D. thesis, Georgia Inst. of Technology, School of M.E., Atlanta, GA, 1993.
13. Halvorson, P. J., Carson, R. J., Jeter, S. M. and Abdel-Khalik, S. I., Critical heat flux limits for a heated surface impacted by a stream of liquid droplets. *ASME Journal of Heat Transfer*, 1994, **116**(3), 679–685.
14. Bockwoldt, T. S., Jeter, S. M. and Abdel-Khalik, S. I., Induced convective enhancement of the critical heat flux for partially heated horizontal flat plates in saturated pool boiling. *ASME Journal of Heat Transfer*, 1992, **114**(2), 518–521.
15. Messana, M. M., Heat transfer to an accelerated stream of droplets impinging onto a heated surface. Masters thesis, Georgia Inst. of Technology, School of M.E., Atlanta, GA, 1991.
16. Rayleigh, Lord, On the instability of jets. *Proceedings of the London Mathematical Society*, Vol. X, London, 1878, pp. 4–13.
17. Lefebvre, A. H., *Atomization and Sprays*. Hemisphere, New York, 1989.
18. Yang, W. J., Theory on vaporization and combustion of liquid drops of pure substances and binary mixtures on heated surfaces. Tech. report 535, Inst. Space Aero. Sci., University of Tokyo, 1975, pp. 423–455.
19. Healy, W. M., Hartley, J. G. and Abdel-Khalik, S. I., Comparison between theoretical models and experimental data for the spreading of liquid droplets impacting a solid surface. *International Journal of Heat and Mass Transfer*, 1996, **39**(14), 3079–3082.